Multiferroic Polymer Laminate Composites Exhibiting High Magnetoelectric Response Induced by Hydrogen-Bonding Interactions

Jiezhu Jin, Fang Zhao, Kuo Han, M. A. Haque, Lijie Dong, and Qing Wang**

The coupling of the magnetic, electric, and elastic properties in multiferroics creates new collective phenomena and enables next-generation device paradigms. In this work, the hydrogen bonding interaction between hydrate salts and ferroelectric polymers is exploited in the development of high-performance magnetoelectric (ME) polymer laminate composites. The microstructures and crystallite structures of the $Al(NO_3)_3{\cdot}9H_2O$ doped poly(vinylidene fluoride-*co*-hexafluoropropylene), P(VDF-HFP), are carefully studied. The effect of hydrogen bonding interaction on the polarization ordering of the ferroelectric polymers is investigated by 2D wide-angle X-ray diffraction, polarized Fourier transform infrared spectra, and dielectric spectra at varied frequencies and temperatures. It is found that hydrogen bond not only promotes the formation of the polar crystallite phase but also improves the polarization ordering in the ferroelectric polymer, which subsequently increases the remnant polarization of the polymers as verified in the polarization-electric field loop measurements. These entail marked improvement in the ME voltage coefficients ($\overline{\alpha}_{ME}$) of the resulting polymer laminate composites based on ferromagnetic Metglas relative to analogous composites. The composite exhibits a state-of-the-art $\overline{\alpha}_{ME}$ value of 20 V cm^{-1} Oe under a dc magnetic field of ≈4 Oe and a colossal $\overline{\alpha}_{ME}$ of 320 V cm^{-1} Oe at a frequency of 68 kHz.

1. Introduction

Multiferroics are a class of multifunctional materials in which at least two of the ferroic order parameters including ferroelectricity, ferromagnetism, and ferroelasticity simultaneously exist.[1,2] The coupling of the magnetic and electric properties opens up a host of new collective phenomena that are absent in each of the individual components, for example, the magnetoelectric (ME) effect, and enables next-generation device paradigms such as multiple-state memory elements, broadband magnetic sensors, electric-field controlled ferromagnetic resonance devices, and actuators.[3–7] The ME effect is defined by an electric polarization in response to an applied magnetic field, or conversely an induced magnetization under an applied electrical field.[8] The ME response was first observed as an intrinsic effect in single-phase crystalline solids such as antiferromagnetic Cr_2O_3 crystals, yttrium iron garnets, boracites, and rare-earth ferrites.[9–11] However, such ME coupling is usually too small to be technologically viable and exists at low temperatures because the Curie temperatures of single phase multiferroics are generally below room temperature. Engineered two-phase composites in which the ferroic components are stress-coupled have been thus developed to overcome the difficulties associated with uniting electrical and magnetic ordering in a single phase.[12,13] The ferrite/piezoelectric ceramic composites, such as $CoFe_2O_4$/$BaTiO_3$, ferrite/lead-zirconate-titanate (PZT), and Tb-Dy-Fe alloys (Terfenol-D)/PZT, have been found to exhibit about two orders of magnitude higher ME response than the mono-phase multiferroics at room temperature.[14–16] By using thin film growing techniques such as molecular beam epitaxy (MBE), epitaxial multiferroic $BaTiO_3$-$CoFe_2O_4$ composites has been synthesized and demonstrated a strong coupling of the order parameters through the hetero-epitaxy of the two lattices.[17,18] Efforts to date have focused primarily on bulk ceramics and ceramic ME composites. However, colossal ME responses have been theoretically predicted in the ferroelectric poly(vinylidene fluoride) (PVDF) based composites, which is attributed to large piezoelectric stress coefficients and great displacement transfer

Dr. J. Jin, K. Han, Prof. Q. Wang
Department of Materials
Science and Engineering
The Pennsylvania State University
University Park, PA, 16802, USA
E-mail: wang@matse.psu.edu
Prof. M. A. Haque
Department of Mechanical
and Nuclear Engineering
The Pennsylvania State University
University Park, PA, 16802, USA
Prof. L. Dong
State Key Laboratory of Advanced Technology
for Materials Synthesis and Processing
Wuhan University of Technology
Wuhan, 430070, China
E-mail: dong@whut.edu.cn
Dr. F. Zhao, Prof. M. A. Haque, Prof. Q. Wang
Materials Research Institute
The Pennsylvania State University
University Park, PA, 16802, USA

DOI: 10.1002/adfm.201301675

capability of the polymer.[19] Indeed, strong ME effect has been experimentally observed in Metglas and Terfenol-D containing ferroelectric polymer laminate composites.[20–25] Multiferroic composites have also been prepared by blending Terfenol-D fillers with ferroelectric poly(vinylidene fluoride-*co*-trifluoroethylene), P(VDF-TrFE), matrix.[26] Compared to the ferroic ceramics, the polymer composites possess additional advantages including easy processing, mechanical flexibility, and ability to be molded into intricate configurations for advanced devices with reduced volume and weight.

In multiferroic composites, the ME effect is a product property of the piezomagnetism, the piezoelectricity of the corresponding phases and their coupling. That is, when a magnetic field is applied to the composites, the ferromagnetic phase deforms because of magnetostriction, and the strain is transferred to the piezoelectric phase, resulting in a change of electric polarization. Accordingly, the ME coefficient can be maximized by tailoring the properties of the ferroelectric and ferromagnetic constituents, and their strain transfer efficiency. While tremendous progress has been made in the ME polymer composites in the last decade, the current strategies mainly utilize the high magnetic permittivity and piezomagnetic coefficients of the magnetostrictive phase to improve the ME coupling,[12,13] with much less attention paid to the optimization of the ferroelectric component.

We describe herein a new approach to high-performance multiferroic polymer composites via utilizing hydrogen bonding interaction to enhance the piezoelectricity of the ferroelectric polymers. It was found that hydrogen bonding not only promoted the formation of the polar β phase and also improved the polarization ordering in the ferroelectric polymer, which subsequently increased the remnant polarization and the piezoelectric coefficient of the polymers and led to one of highest ME voltage coefficients among the known multiferroic materials.

2. Results and Discussion

2.1. Ferroelectric Polymer Films

Poly(vinylidene fluoride-*co*-hexafluoropropylene), P(VDF-HFP) (10 wt% HFP), was employed as the piezoelectric phase in the composites. Different from the typical ferroelectric polymers such as PVDF and its copolymer with trifluoroethylene (TrFE) whose transverse piezoelectric coefficient d_{31} is about half of the longitudinal piezoelectric coefficient d_{33}, P(VDF-HFP)s exhibit an unusual piezoelectric response, that is, $|d_{31}/d_{33}| > 1$.[27] This makes P(VDF-HFP) particularly desirable in the laminate multiferroic composites operated in longitudinally (L) magnetized and transversely (T) poled (or L–T) mode. The crystalline β phase that accounts for the ferroelectric and piezoelectric properties of the PVDF based ferroelectric polymers has been conventionally obtained by casting from polar solutions, stretching process, and fast quenching from the melt state.[28–32] In this study, $Al(NO_3)_3 \cdot 9H_2O$ (8 wt%) was added in the *N*,*N*-dimethylformamide (DMF)/acetone (1:1 v/v) solution of P(VDF-HFP). The concentration of the salt in the polymer was optimized according to previous studies.[33] It was found that, when the salt content was higher than 8 wt%, the aggregated salt led to high leakage currents and thus made it difficult to polarize the ferroelectric polymer under electric field.

The cast ferroelectric polymer films were dried at 135 °C under vacuum and then rapidly quenched in liquid nitrogen, followed by uniaxially stretching at 135 °C with a draw ratio ($L_{final}/L_{initial}$) of 4 to yield the films denoted as **P2**. For the purpose of comparison, the pristine P(VDF-HFP) was processed under the same condition and referred to as **P1**. **P2** was further annealed at 110 °C for 3 h to produce the films named as **P3**. The typical thickness of the films was ≈~15 μm.

2.2. Microstructures and Crystallite Structures

As shown in **Figure 1**a, the presence of hydrogen bonding interaction between O–H from the $Al(NO_3)_3 \cdot 9H_2O$ salt and C–F from P(VDF-HFP), where fluorine acts as an hydrogen

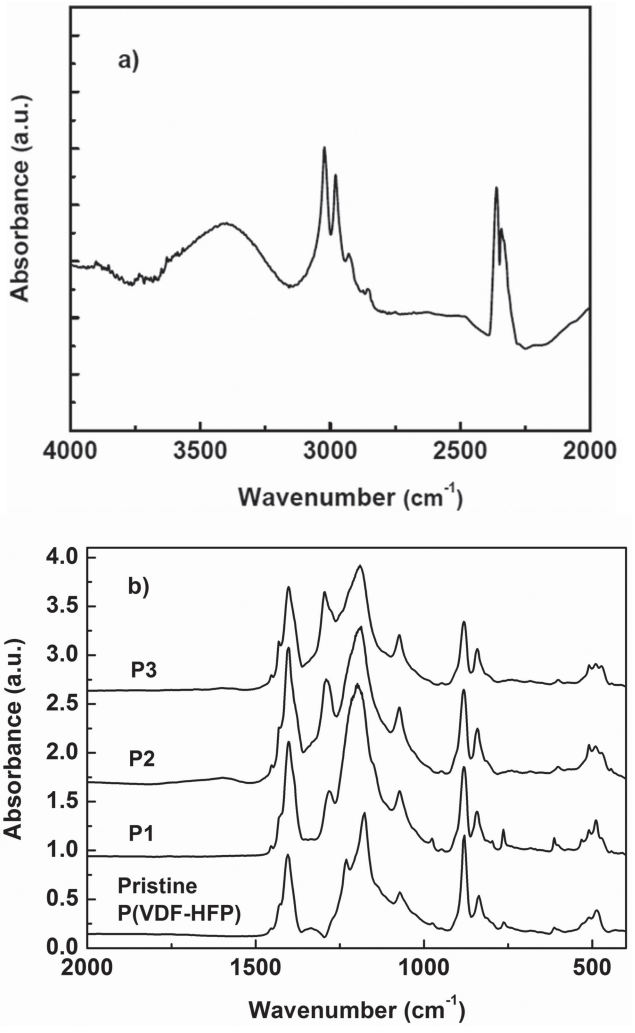

Figure 1. FTIR spectra of a) the $Al(NO_3)_3 \cdot 9H_2O$ hydrated samples (**P2** and **P3**) in the wavenumber range of 2000–4000 cm^{-1} and b) the polymer films in the wavenumber range of 400–2000 cm^{-1}.

Table 1. Fractions of all-trans, TG, and T_3G conformations calculated from the FTIR spectra of P(VDF-HFP).

P(VDF-HFP)	$F_{m>4}$	F_{TG}	F_{T3G}
Pristine	0.15	0.59	0.26
P1	0.62	0.26	0.12
P2	0.77	0.10	0.13
P3	0.82	0.07	0.1

bond acceptor, was clearly manifested by the emergence of a broad absorption band centered at 3400 cm^{-1} in the Fourier transform infrared (FTIR) spectra of the $Al(NO_3)_3 \cdot 9H_2O$ doped P(VDF-HFP) films **P2** and **P3**.[33,34] C–H stretching vibrations of P(VDF-HFP) were located at 3019 and 2971 cm^{-1}. The characteristic peaks of P(VDF-HFP), that is, CH_2 wagging [$\omega(CH_2)$], antisymmetric CF_2 stretch [$\nu_a(CF_2)$] and CF_3 out-of-plane deformation [$\gamma(CF_3)$] absorbed IR radiation at 1400, 1189, and 1064 cm^{-1}, respectively. The absorption bands at 510, 614 and 1288 cm^{-1} shown in Figure 1b were assigned to the vibration of the CF_2 group for trans-gauche (T_3G), TG, and all-trans ($T_{m>4}$) chain conformations, respectively, of the polymers.[35] Their relative intensities were used to evaluate the relative γ, α, and β contents in the films according to the following equation:[36]

$$F_i = \frac{A_i}{A_I + A_{II} + A_{III}} \quad (1)$$

where i = I, II, and III, A_I, A_{II}, and A_{III} are the absorbance of crystal forms I, II, and III, that is, all-trans, T_3G, and TG sequences, respectively, and F_i is the fraction of chain sequence i. The result is presented in **Table 1**. As expected, fast quenching and mechanical drawing induced the transformation from the non-polar α phase that was dominant in the pristine P(VDF-HFP) to the polar β phase in **P1**. The fraction of the β phase was further increased from 0.62 of **P1** to 0.77 and 0.82 of films **P2** and **P3**, respectively, indicating that the addition of hydrate and subsequent annealing favored the crystallization of the β phase.

Consistent with the FTIR results, the characteristic peaks at 20.3° and 36.5° attributable to the (110, 200) and (020) diffractions, respectively, of the crystalline β phase[37] became increasingly pronounced from the films **P1** to **P3** in the wide-angle X-ray diffraction (WXRD) spectra as shown in **Figure 2**. Concomitantly, the intensities of the diffractions at 17.6°, 18.5°, and 26.6° originated from the (100), (020), and (120) planes, respectively, of the nonpolar α phase were reduced progressively from **P1** to **P2** and **P3**. The crystalline and amorphous regions shown in the XRD patterns were separated by using the Gaussian function to calculate crystallinity. The size of crystallites was determined according to the Scherrer formula:

$$t = \lambda / B \cos \theta_B \quad (2)$$

where t is the crystallite size, B is the normalized full width at half maximum of the diffraction peak, λ is the X-ray wavelength (1.54 Å) and $2\theta_B$ is the diffraction angle corresponding to the Bragg maximum. As summarized in **Table 2**, the crystallinity of the polymer was increased from 67% of **P1** to 75% of **P2** and 80% of **P3**. Concurrently, the crystallite size of the β phase was improved from 5.4 nm of **P1** to 5.7 nm of **P2** and 6.5 nm of **P3**.

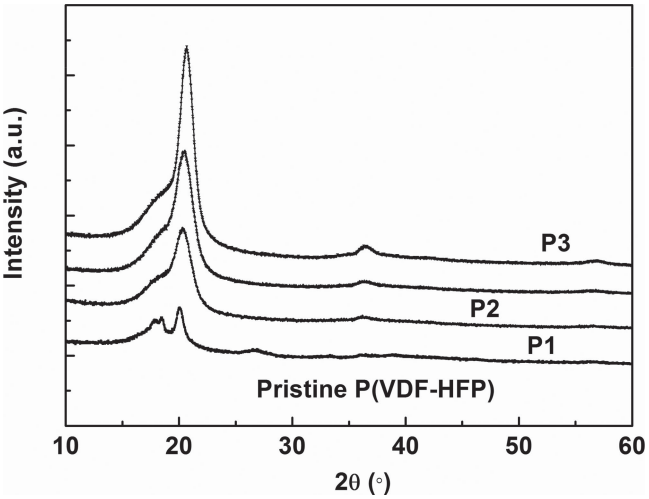

Figure 2. XRD patterns of the P(VDF-HFP) samples.

In agreement with the trends observed in the WXRD and FTIR studies, a systematic increase of melting temperature from 148 to 150 °C, accompanied by an associated improvement in the heat of fusion (ΔH_m) from 33.7 to 39.3, and 41.6 J g^{-1} was found from **P1** to **P2** and **P3**, respectively in the DSC measurements. These results could be rationalized that the hydrogen bonding interactions between the salts and P(VDF-HFP) result in the interchain registration of the all-trans conformations, which consequently function as nucleation sites to improve the crystallinity and crystallite size and the content of the polar β phase of the polymer from the films **P1** to **P2** and **P3**.[38]

2.3. Polarization

In addition to the crystalline phase, polarization ordering is known to play an equally important role on the ferroelectric and piezoelectric properties of the ferroelectric polymer.[33,39] As a result of anisotropic orientational polarizability of PVDF crystals, the films with the crystal *c*-axes perpendicular to the electric field exhibit larger maximum/remnant polarization and accordingly, higher electromechanical properties as compared to the films with randomly oriented crystals. **Figure 3**a shows 2D WXRD patterns of the polymer films. The pristine

Table 2. The crystallinity, crystalline size and d-spacing calculated from X-ray diffraction patterns of P(VDF-HFP).

P(VDF-HFP)	Crystallinity [%]	Crystal Size [nm]	d-spacing [Å]
Pristine	59.7	11.8 (α)	4.41
P1	67.8	5.4 (β)	4.33
P2	75.5	5.7 (β)	4.32
P3	80.2	6.5 (β)	4.28

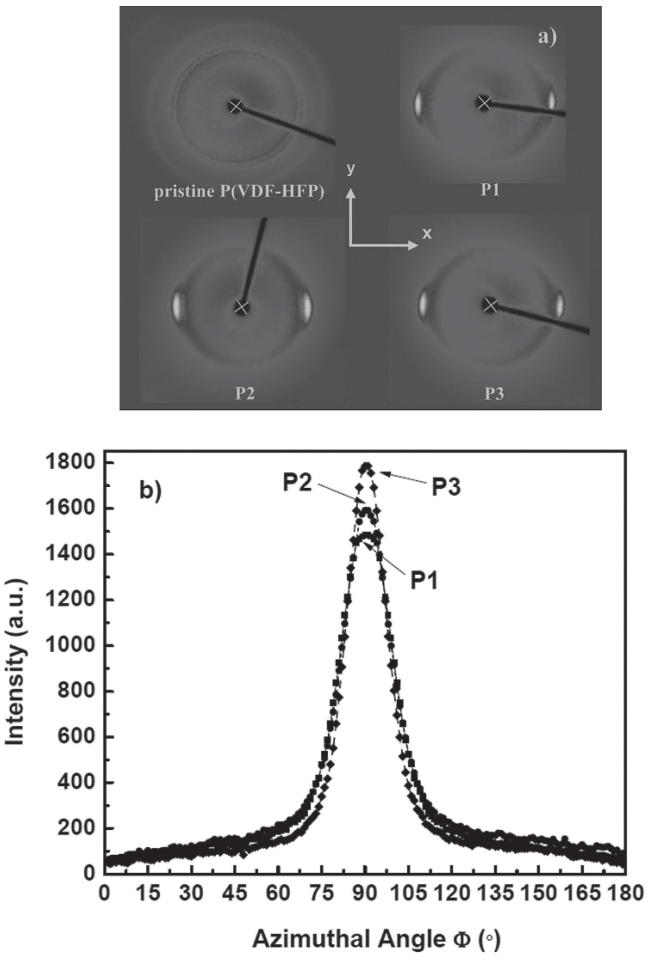

Figure 3. a) 2D WAXD patterns of P(VDF-HFP) films. The X-ray beam was directed normal to the film surface. The film is in *x*–*y* plane with the stretching direction along the y axis. b) Azimuthal angle distribution of XRD intensity of composite (110/200) plane of the β phase of **P1**, **P2**, and **P3** films, respectively. Azimuthal angle at 0° corresponds to the stretching direction (*y* axis) and the reference direction to calculate Hermen's orientation parameter, and azimuthal angle at 90° is perpendicular to the stretching direction (*x* axis) in the film plane.

P(VDF-HFP) films exhibited sharp isotropic rings, indicative of a random orientation of the crystals with respect to the normal direction of the film. For **P1**, **P2**, and **P3**, the *c*-axes of the β phase crystalline regions were preferentially oriented parallel to the drawing direction (*y*) because the $(110/200)_\beta$ reflection appeared in the horizontal *x* direction in the *z* 2-dimension wide-angle X-ray diffraction (2D WAXD) pattern. Since the direction of the polarizing electric field is perpendicular to the film surface, this crystallite distribution orientation favors dipole alignment and consequently, polarization and piezoelectricity of the film. The azimuthal angle dependence of the WXRD peak intensity of the β phase at (110/200) plane is displayed in Figure 3b. The Herman's orientation function, *f*, a quantitative sign of chain and crystalline orientation in a polymer with anisotropic crystalline structure, can be determined according to the following equations:[40]

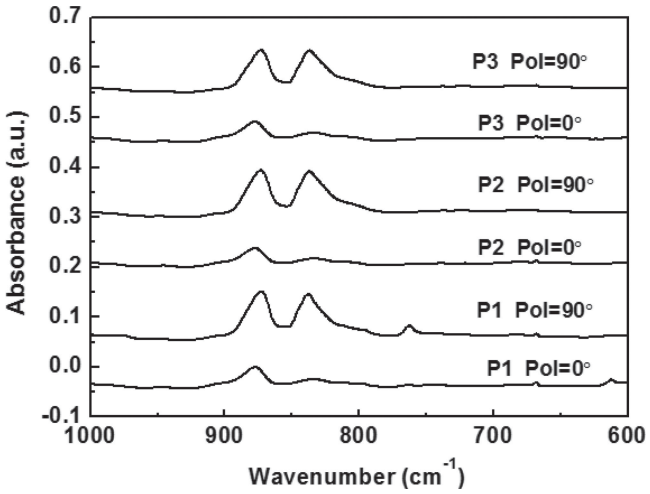

Figure 4. Polarized FTIR spectra of **P1**, **P2** and **P3** films with polarizer set at 0° and 90°.

$$f = \frac{3 < \cos^2 \phi > -1}{2} \tag{3}$$

with

$$< \cos^2 \phi > = \frac{\int_0^{\frac{\pi}{2}} I(\phi) \cos^2 \phi \sin \phi \, d\phi}{\int_0^{\frac{\pi}{2}} I(\phi) \sin \phi \, d\phi} \tag{4}$$

where Φ is the azimuthal angle that is the angle between the normal of the crystallographic plane and the reference direction in the film plane and $I(\Phi)$ is the intensity as a function of azimuthal angle. *f* varies from 0 for random orientation to 1 for perfect orientation along the reference axis or –0.5 for perpendicular orientation relative to the reference axis. It was found that *f* was increased from –0.30 of **P1** to –0.33, and –0.35 of **P2** and **P3**, respectively, signifying the improvement of the crystalline chain orientation by hydrogen bonding and post-annealing. We hypothesize that the hydrogen bonded O–H group (O–H···F–C) increases the stability of the molecular chain orientation after stretching, leading to better alignment of dipoles.

To further quantify the chain orientation, the dichroic ratio (DR) of the polarized FTIR spectra shown in **Figure 4** was calculated according to:

$$\text{D.R.} = \frac{I_T - I_{//}}{I_T + I_{//}} \tag{5}$$

where I_T and I_{ll} are the intensities of the FTIR absorption bands perpendicular (90°) and parallel (0°) to the polarizer direction, respectively. The DR value ranges from 0 for random orientation to 1 for perfect orientation. The peak at 880 cm^{-1} is assigned to the vibration of CH_2 rocking and CF_2 asymmetric stretching and rocking in the α-phase, while the 842 cm^{-1} band is characteristic of CF_2 symmetric stretching in the β-phase.[41] The presence of stronger absorption bands at 842 and 880 cm^{-1} when polarizer was placed at 0° indicated that the polar *b* axis of the P(VDF-HFP) copolymer chain was perpendicular to the

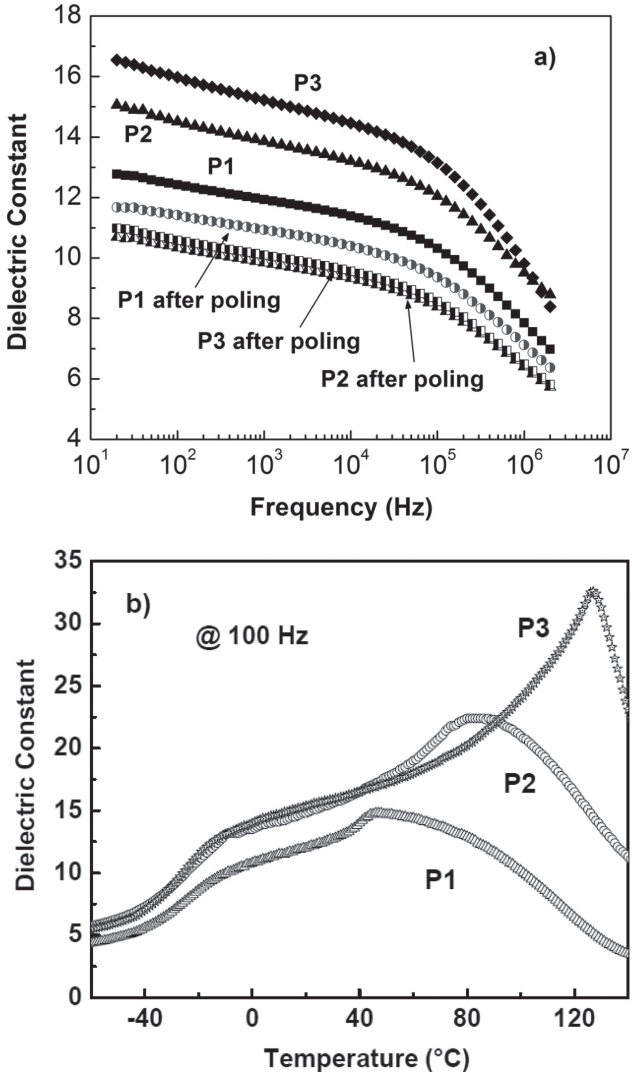

Figure 5. a) Frequency dependence of the dielectric constant of the films before and after poling. b) Temperature dependence of the dielectric constants of the films measured at 100 Hz.

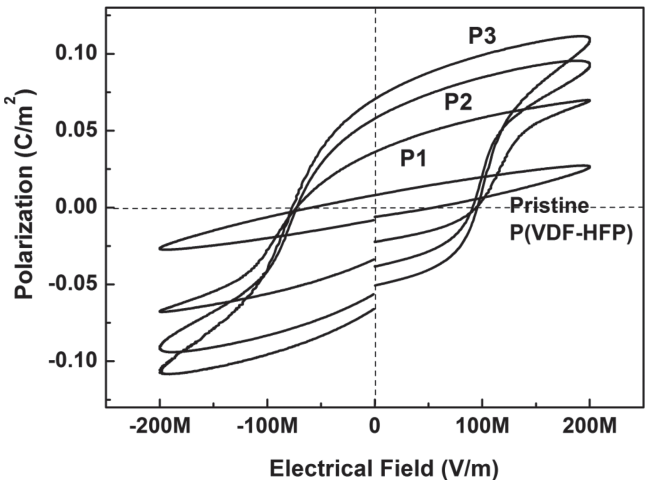

Figure 6. *P–E* loops of the P(VDF-HFP) films measured at 200 MV m^{-1}.

film surface and the planar zigzag chains were aligned parallel to the film surface. The DR values were found to increase monotonously from 0.6 of **P1** to 0.72 and 0.74 of **P2** and **P3**, respectively, at 842 cm^{-1} and from 0.35 of **P1** to 0.44 and 0.48 of **P2** and **P3**, respectively, at 880 cm^{-1}, clearly manifesting that higher degrees of chain orientation were achieved by hydration and post-annealing in **P2** and **P3**.

The enhancement of polarization ordering induced by hydrogen-bonding interaction has also been substantiated in the frequency dependence of the dielectric constant of the polymer films. As show in **Figure 5**a, the dielectric constants of the polymers measured along the poling direction were reduced after poling due to the alignment of the dipoles along the direction of the applied field. The dielectric constant of **P1** measured at 1 kHz decreased from 11.9 to 10.9 after poling under 200 MV m^{-1} for 5 min. at room temperature. Comparatively, the dielectric constants of **P2** and **P3** at 1 kHz were reduced from 13.9 to 9.8 and from 15.2 to 10.1, respectively, after poling under the same condition. A more pronounced reduction in the dielectric constant upon poling suggests that **P2** and **P3** films possess a better alignment of dipoles and polarization ordering.[42] Additionally, it is evident from the dielectric relaxation spectra shown in Figure 5b that the peak corresponding to the transition from the polar to nonpolar phases shifted progressively from approximately 44 °C in **P1** to 82 °C in **P2** and 127 °C in **P3**, again verifying the existence of higher ordering of the polar phase in **P2** and **P3**.[43]

Figure 6 compares the polarization-electric field (*P–E*) loops of the films measured at 200 MV m^{-1} using a modified Sawyer-Tower circuit. Typical ferroelectric *P–E* loops characterized with hysteresis and remnant polarization (P_r) have been observed in the films. Compared to the pristine P(VDF-HFP) with a P_r of 15 mC m^{-2}, **P1** exhibited an improved P_r value of 47 mC m^{-2}. P_r was increased markedly to 78 and 87 mC m^{-2} in **P2** and **P3**, respectively, originating from the constant increase in the polar β phase and the polarization ordering from **P1** to **P2** and **P3**. Analogously, the increase of storage modulus measured by dynamic mechanical analysis (DMA) from 1.26 GPa of **P1** to 1.66 and 1.87 GPa of **P2** and **P3**, respectively, is well correlated with the enhancement of crystallinity, crystallite size and chain orientation. Since the piezoelectric coefficient is directly proportional to the remnant polarization in the PVDF based ferroelectric polymers, higher piezoelectricity was thus anticipated in **P2** and **P3** (see the discussion below).[44]

2.3. Multiferroic and Piezoelectric Properties

The multiferroic laminate composites were fabricated by attaching the transversely poled P(VDF-HFP) films on the central part of iron-based Metglas sheet to take advantage of the magnetic flux concentration effect. Metglas was chosen as the magnetostrictive layer due to its high piezomagnetic coefficient ($\approx 4 \times 10^{-6}$ Oe^{-1}).[45] **Figure 7**a presents the dependence of the ME voltage coefficient α_{ME} on dc magnetic fields (H_{dc}) for the laminate composites measured at 20 Hz. Negligible output voltage was detected in the pristine P(VDF-HFP)-Metglas

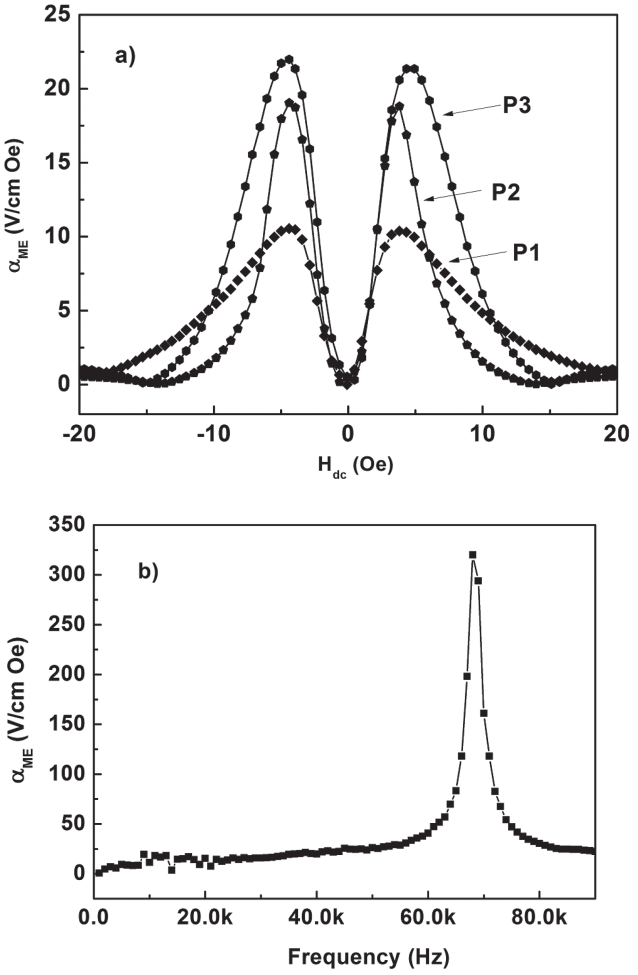

Figure 7. a) ME voltage coefficient of the composites as a function of dc magnetic field. b) ME voltage coefficients of the **P3**-Metglas composite at varied frequencies.

composites. For the **P1**–Metglas composites, a α_{ME} value of 10.5 V cm^{-1} Oe was obtained, which was increased to 19.1 and 22 V cm^{-1} Oe for **P2** and **P3** based composites, respectively. The achieved α_{ME} are compared favorably to the values of the reported multiferroic polymer composites. For example, the P(VDF-TrFE) based composites exhibit the maximum value of α_{ME} of 6.9 V cm^{-1} Oe, and the α_{ME} of Metglas/PVDF and Terfenol-D/PVDF composites are 7.2 and 3 V cm^{-1} Oe, respectively.[12,20] It is important to note that the prepared composites required an applied magnetic field of only ≈4 Oe to achieve a maximum ME coefficient, which is more than 50% lower than the magnetic bias of the PVDF/Metglas laminates.[24] A low magnetic bias field is highly desirable for highly sensitive magnetic sensors and miniaturized transducers. The frequency dependence of the α_{ME} of **P3**–Metglas composite is presented in Figure 7b. A colossal α_{ME} of 320 V cm^{-1} Oe was obtained at a frequency of 68 kHz, which is attributed to the electromechanical resonance enhancement of elastic coupling interaction between the P(VDF-HFP) and Metglas layers.

The laminated ME composites represent a serial combination of the magnetostrictive and piezoelectric layers, where the intrinsic transverse piezoelectricity of the poled P(VDF-HFP) implies a linear relationship between the induced transverse electrical polarization and the longitudinal stress. According to the equivalent circuit method, the ME voltage coefficient can be expressed as:[46]

$$\alpha_{ME} = \frac{\partial E}{\partial H} = \frac{n d_{33,m} d_{31,p}}{n\varepsilon_0 \varepsilon_{33}^S s_{11}^E + (1-n) s_{33}^H (\varepsilon_0 \varepsilon_{33}^S + d_{31,p}^2 / s_{11}^E)} \quad (6)$$

where n is the magnetic phase thickness ratio, s_{11}^E and s_{33}^H are the elastic compliances of the piezoelectric and magnetostrictive layers, respectively, ε_0 is the vacuum permittivity, ε_{33}^S is the dielectric constant of the piezoelectric material at constant strain, and $d_{33,m}$ and $d_{31,p}$ are the longitudinal magnetostriction and transverse piezoelectric strain coefficients, respectively. While it is rather difficult to unambiguously determine d_{31} of the thin films in the experiments, the effective d_{31} can be estimated according to Equation 6. Based on the measured α_{ME}, dielectric constant and elastic moduli, and the magnetostrictive coefficient found in the literature,[20] the effective d_{31} was assessed to be approximately 18.4, 25.8, and 28.6 pC/N for **P1**, **P2** and **P3**, respectively. Interestingly, these values are greater than those of uniaxially stretched PVDF and P(VDF-TrFE) whose d_{31} are typically around 18 and 10 pC/N, respectively.[47]

3. Conclusions

In summary, the hydrogen bonding interaction between hydrate salts and ferroelectric polymers was exploited in the design of high-performance ME composites. The effect of hydrogen bonds on the polarization ordering of the ferroelectric polymers was investigated by 2D WXRD, polarized FTIR, and dielectric relaxation spectra. The increase of chain orientation, coupled with the expected enhancement of the evolution of the polar phase of the ferroelectric polymers stemming from hydrogen-bonding interactions, entails marked improvement in the ME voltage coefficients relative to analogous composites. Additionally, the notably low dc bias requirement is an important advantage of the prepared composites over the previously reported ME materials. The simplicity and scalability of the described method further suggest their potential in practical applications. We expect this work presents a promising direction to enhance the electromechanical and ferroelectric properties of the electroactive polymers for the multifunctional composites exhibiting collective properties and functionalities.

4. Experimental Section

Preparation of Ferroelectric Polymer Films: P(VDF-HFP) (10 wt.% HFP, Knyar 2801, Arkema) solutions were prepared by dissolving P(VDF-HFP) powder in DMF/acetone (1:1 v/v) with or without addition of 8 wt% of $Al(NO_3)_3 \cdot 9H_2O$ (99.995%). The thin films were deposited through a solution-casting process on glass slide. The as-cast films were dried at 135 °C for 12 h under vacuum. The samples were quenched by immersing them in liquid nitrogen for 15 min, and followed by uniaxially stretching by means of a narrow zone drawing process, with the temperature of the heating zone at 135 °C. The stretching ratio is fixed at 4. After stretching, some of the samples were annealed at 110 °C for 3 h.

Preparation of ME Laminate Composites: The P(VDF-HFP) films were sputtered with 50 nm thick gold on both sides of surface as electrodes

and transversely poled by a 200 MV m^{-1} constant electrical field at room temperature for 5 min. Iron-based Metglas 2605 SA1 (Metgals, Inc., Conway, SC) and poled P(VDF-HFP) thin film layers were glued using a thin layer of commercial available epoxy to obtain the two-layer ME laminates. The thickness of Metglas layer is 25 μm. The length of Metglas sheet is 30 mm, and the width is 4.5 mm. P(VDF-HFP) layers are fixed at 7 mm long and 4 mm wide, attached on the central part of the Metglas sheets.

Structure Characterization: The thermal transition data were obtained by a TA Instruments Q100 differential scanning calorimeter (DSC) at a heating and cooling rate of 10 °C min^{-1}. Dynamic mechanical analysis (TA DMA 2980) was carried out to investigate the elastic modulus of the P(VDF-HFP) films at 1 Hz. The crystalline and microstructure of the copolymers was characterized by FTIR spectroscopy (Nicolet 510) and WXRD (Scintag CuKα diffractormeter with a X-ray wavelength of 1.54 Å).

Dielectric and ME Property Measurement: The weak field dielectric constant and loss tangent of the P(VDF-HFP) copolymer films were measured by an Agilent E4980A LCR meter from 20 Hz to 2 MHz. Temperature dependence of the dielectric constant at frequencies ranging from 10^2 to 10^6 Hz were characterized using a HP LCR meter (4284A) equipped with a Delta Design Oven (Model 2300). The polarization-electrical field (*P*–*E*) hysteresis loops were measured using the modified Sawyer-Tower circuits, and the ac field used has a sinusoidal waveform with a frequency of 1 Hz. To measure the ME coupling coefficients of the laminates, dc (H_{dc}) and ac (H_{ac}) magnetic fields were applied along the length of the laminates. At 20 Hz frequency, an electromagnet was used to provide H_{ac} and H_{dc} at H_{ac} = 0.724 Oe. At frequency larger than 20 Hz, Helmholtz coils were used to generate H_{ac} and H_{dc}. A function generator generated a controllable input current to the electromagnet or Helmholtz coil, and a lock-in amplifier was used to measure the output voltage induced across the P(VDF-HFP) layer of the ME laminates.

Acknowledgements

This work was supported by the ACS Petroleum Research Fund (Q.W.) and the Center for Nanoscale Mechatronics & Manufacturing of the Korea Institute of Machinery & Materials (M.A.H.). L.D. acknowledges financial support by the National Nature Science Foundation of China (No. 51273157) and Program for New Century Excellent Talents in University (NCET-10–0659).

Received: May 16, 2013
Revised: August 19, 2013
Published online: September 20, 2013

[1] W. Eerenstein, N. D. Mathur, J. F. Scott, *Nature* **2006**, *442*, 759.
[2] N. A. Spaldin, S. W. Cheong, R. Ramesh, *Phys. Today* **2010**, *63*, 38.
[3] I. Levin, J. Li, J. Slutsker, A. L. Roytburd, *Adv. Mater.* **2006**, *18*, 2044.
[4] J. Das, Y. Y. Song, N. Mo, P. Krivosik, C. E. Patton, *Adv. Mater.* **2009**, *21*, 2045.
[5] N. Hur, S. Park, P. A. Sharma, J. S. Ahn, S. Guha, S. W. Cheong, *Nature* **2004**, *429*, 392.
[6] S. M. Wu, S. A. Cybart, P. Yu, M. D. Rossell, J. Zhang, R. Ramesh, R. C. Dynes, *Nat. Mater.* **2010**, *9*, 756.
[7] Y. Wang, D. Gray, D. Berry, J. Gao, M. Li, J. Li, D. Viehland, *Adv. Mater.* **2011**, *23*, 4111.
[8] M. Fiebig, *J. Phys. D Appl. Phys.* **2005**, *38*, R1.
[9] V. J. Folen, G. T. Rado, E. W. Stalder, *Phys. Rev. Lett.* **1961**, *6*, 607.
[10] W. Prellier, M. P. Singh, P. Murugavel, *J. Phys.: Condensed Matter.* **2005**, *17*, R803.
[11] A. K. Pradhan, K. Zhang, D. Hunter, J. B. Dadson, G. B. Loutts, P. Bhattacharya, R. Katiyar, J. Zhang, D. J. Sellmyer, U. N. Roy, Y. Cui, A. Burger, *J. Appl. Phys.* **2005**, *97*, 093903.
[12] J. Ma, J. M. Hu, Z. Li, C. W. Nan, *Adv. Mater.* **2011**, *23*, 1062.
[13] G. Srinivasan, *Annu. Rev. Mate. Res.* **2010**, *40*, 153.
[14] C. A. F. Vaz, J. Hoffman, C. H. Ahn, R. Ramesh, *Adv. Mater.* **2010**, *22*, 2900.
[15] J. Ryu, S. Priya, A. V. Carazo, K. Uchino, H. E. Kim, *J. Amer. Ceramic Soc.* **2001**, *84*, 2905.
[16] S. Dong, J. F. Li, D. Viehland, J. Cheng, L. E. Cross, *Appl. Phys. Lett.* **2004**, *85*, 3534.
[17] J. Wang, J. B. Neaton, H. Zheng, V. Nagarajan, S. B. Ogale, B. Liu, D. Viehland, V. Vaithyanathan, D. G. Schlom, U. V. Waghmare, N. A. Spaldin, K. M. Rabe, M. Wuttig, R. Ramesh, *Science* **2003**, *299*, 1719.
[18] J. H. Lee, L. Fang, E. Vlahos, X. Ke, Y. W. Jung, L. F. Kourkoutis, J. W. Kim, P. J. Ryan, T. Heeg, M. Roeckerath, V. Goian, M. Bernhagen, R. Uecker, P. C. Hammel, K. M. Rabe, S. Kamba, J. Schubert, J. W. Freeland, D. A. Muller, C. J. Fennie, P. Schiffer, V. Gopalan, E. Johnston-Halperin, D. G. Schlom, *Nature* **2010**, *466*, 954.
[19] C. W. Nan, M. Li, J. H. Huang, *Phys. Rev. B* **2001**, *63*, 144415.
[20] J. Zhai, S. Dong, Z. Xing, J. Li, D. Viehland, *Appl. Phys. Lett.* **2006**, *89*, 083507.
[21] K. Mori, M. Wuttig, *Appl. Phys. Lett.* **2002**, *81*, 100.
[22] S. Dong, J. Zhai, J. Li, D. Viehland, *Appl. Phys. Lett.* **2006**, *89*, 252904.
[23] Y. Lin, N. Cai, J. Zhai, G. Liu, C. W. Nan, *Phys. Rev. B* **2005**, *72*, 012405.
[24] J. Jin, S. Lu, C. Chanthad, Q. Zhang, M. A. Haque, Q. Wang, *Adv. Mater.* **2011**, *23*, 3853.
[25] S. G. Lu, J. Z. Jin, X. Zhou, Z. Fang, Q. Wang, Q. M. Zhang, *J. Appl. Phys.* **2011**, *110*, 104103.
[26] Z. Shi, C. W. Nan, T. M. Liu, D. A. Filippov, M. I. Bichurin, *Phys. Rev. B* **2004**, *70*, 134417.
[27] B. Neese, Y. Wang, B. Chu, K. Ren, S. Liu, Q. M. Zhang, C. Huang, J. West, *Appl. Phys. Lett.* **2007**, *90*, 242917.
[28] K. Tashiro, Crystal Structure and Phase Transition of PVDF and Related Copolymers in *Ferroelectric Polymers, Chemistry, Physics, and Applications*, (Ed: H. S. Nalwa), Dekker, New York **1995**, pp 63–182.
[29] M. Wegener, W. Künstler, K. Richter, R. Gerhard-Multhaupt, *J. Appl. Phys.* **2002**, *92*, 7442.
[30] X. He, K. Yao, B. K. Gan, *J. Appl. Phys.* **2005**, *97*, 084101.
[31] H. J. Jung, J. Chang, Y. J. Park, S. J. Kang, B. Lotz, J. Huh, C. Park, *Macromolecules* **2009**, *42*, 4148.
[32] K. Koga, N. Nakano, T. Hattori, H. Ohigashi, *J. Appl. Phys.* **1990**, *67*, 965.
[33] X. He, K. Yao, *Appl. Phys. Lett.* **2006**, *89*, 112909.
[34] M. Falk, O. Knop, in *Water: A Comprehensive Treatise*, (Ed: F. Franks), Plenum, New York **1973**, Vol. *2*, p 55.
[35] M. A. Bachmann, W. L. Gordon, J. L. Koenig, J. B. Lando, *J. Appl. Phys.* **1979**, *50*, 6106.
[36] S. Osaki, Y. Ishida, *J. Polym. Sci. B: Polym. Phys.* **1975**, *13*, 1071.
[37] Y. Lu, J. Claude, Q. M. Zhang, Q. Wang, *Macromolecules* **2006**, *39*, 6962.
[38] M. Benz, W. B. Euler, O. J. Gregory, *Macromolecules* **2002**, *35*, 2682.
[39] F. Guan, J. Pan, J. Wang, Q. Wang, L. Zhu, *Macromolecules* **2010**, *43*, 384.
[40] M. C. Branciforti, V. Sencadas, S. Lanceros-Mendez, R. Gregorio, *J. Polym. Sci. B: Polym. Phys.* **2007**, *45*, 2793.
[41] N. M. Reynolds, K. J. Kim, C. Chang, S. L. Hsu, *Macromolecules* **1989**, *22*, 1092.
[42] G. T. Davis, T. Furukawa, A. J. Lovinger, M. G. Broadhurst, *Macromolecules* **1982**, *15*, 329.
[43] Y. Lu, J. Claude, L. E. Norena-Franco, Q. Wang, *J. Phys. Chem. B* **2008**, *112*, 10411.
[44] T. Furukawa, *IEEE Trans. Electr. Insul.* **1989**, *24*, 375.
[45] J. Zhai, Z. Xing, S. Dong, J. Li, D. Viehland, *J. Am. Ceram. Soc.* **2008**, *91*, 351.
[46] S. Dong, J. F. Li, D. Viehland, *IEEE Trans. Ultrason. Ferroelect. Freq. Control* **2003**, *50*, 1253.
[47] *Ferroelectric Polymers*, (Ed: H. S. Nalwa), Marcel Dekker, New York **1995**.